CHAPTER 88

Topographical Change around Multiple Large Cylindrical Structures under Wave Actions

Chang–Je KIM[1], Koichiro IWATA[2], Yoshihito MIYAIKE[3] and Hong–Sun YU[4]

Abstract

This paper is aimed to investigate theoretically and experimentally the topographical change and the local scouring around multiple large cylindrical structures under wave actions. It is revealed from laboratory experiments that the bottom configuration, the local scouring area and its depth around the cylindrical structures are changed largely according to the number of cylindrical structures, the structure's diameter, the incident wave angle and the sediment size. The theoretical model which developed newly is shown to predict well the topographical change around the structures.

1. Introduction

Cylindrical structures are one type of the widely-used coastal and offshore structures such as large volumed gravity platforms or water intake towers for power plants. Very recently, multiple large cylindrical structures have been constructed in shallow water depth and have been reported to suffer from local scouring around the cylindrical structures under wave actions in Japan. It goes without saying that the prediction of topographical change and the evaluation of local scouring area and depth around structures are indispensable for safety design of the structures. The accumulated knowledge of bottom topographical change around multiple large cylinders is, however, little compared with that of one large cylinder or small cylinders.

[1]Lecturer, Korea Maritime University, Busan, 606–791, KOREA
[2]Professor, Nagoya University, Nagoya 464-01, JAPAN
[3]General Manager, Chubu Electric Power Co. Ltd., Nagoya 461, JAPAN
[4]Professor, Korea Maritime University, Busan, 606–791, KOREA

This paper is to discuss theoretically and experimentally the bottom to-
pographical change and local scouring around the two or three large cylinders
under wave actions. First, the theoretical model is newly developed to evaluate
the topographical change and to predict the scouring area and depth. Next,
elaborate laboratory experiments are conducted to investigate the change of
bottom configuration due to changes of the number of the large cylinders, their
diameters, the incident wave and angle, and the sediment size. Comparing with
laboratory experiments, the theoretical model proposed in this paper is shown
to be very useful to evaluate the bottom topographical change and the local
scouring around multiple large cylindrical structures.

2. Theoretical model

2.1 Diffraction theory

The diffraction theory is applied to evaluate the wave kinematics and wave
deformation around the circular cylinders, since the ratio of the cylinder's di-
ameter to the wavelength(diffraction parameter), D/L is more than 0.2. The
source distribution function method using a vertical line wave source Green's
function(Issacson, 1978) is employed in this paper under the assumptions of
inviscid and incompressible fluid, and irrotational wave motion. The water
particle velocities can be described with velocity potential $\Phi(= \Phi_I + \Phi_S; \Phi_I$
is the incident velocity potential, Φ_S the scattered velocity potential), which
satisfies Laplace equation. Φ, Φ_I, and Φ_S are all functions of x, y, z, and t, and
(x, y, z) are the Cartesian coordinates of a point in the fluid field at which the
potentials(Φ, Φ_I, and Φ_S) are calculated at time t. When it is assumed that
the wave height is sufficiently small for linear wave theory to apply, the incident
wave velocity potential Φ_I is a known value, and the scattered wave velocity
potential Φ_S is obtained from the source distribution function method(see, Kim
and Iwata, 1993).

The wave height H around structures is given as

$$H = 2\left|\frac{i\sigma}{g}\left\{\phi_I(x,y) + \phi_S(x,y)\right\}\right| \tag{1}$$

where $i = \sqrt{-1}$, σ denotes the wave angular frequency, g the gravitational
acceleration, ϕ_I the complex amplitude of the incident velocity potential Φ_I,
ϕ_S the complex amplitude of the scattered velocity potential Φ_S, and $|\ \ |$ the
absolute value.

The water particle velocities $U_b(x, y; t)$, $V_b(x, y; t)$ in the x-, y- directions near bottom around structures are as follows, respectively.

$$U_b = \text{Real}[\frac{\partial \Phi}{\partial x}|_{z=-h}] = \text{Real}[U_0(x, y) \exp(-i\sigma t)] \tag{2}$$

$$V_b = \text{Real}[\frac{\partial \Phi}{\partial y}|_{z=-h}] = \text{Real}[V_0(x, y) \exp(-i\sigma t)] \tag{3}$$

in which Real denotes the real part of the expression following, h the still water depth, U_0 and V_0 are the complex amplitudes of U_b and V_b, respectively.

It has been reported that the wave height and the bottom velocity evaluated with the source distribution function method using a vertical line wave source Green's function, were in good agreement with those by experiments(Kim and Iwata, 1993, Kim et al., 1994).

2.2 Mass transport velocity

Taking constant viscosity into account, Lagrangian mass transport velocities $\overline{u_L}$, $\overline{v_L}$ in the x-, y- directions in the bottom boundary layer combined Stokes' mean drift with Eulerian mean drift are given as(Carter et al.,1973)

$$\overline{u_L} = \frac{1}{4\sigma}\text{Real}\left\{F_5 U_0\frac{\partial U_0^*}{\partial x} + F_6 V_0\frac{\partial U_0^*}{\partial y} + F_7 U_0\frac{\partial V_0^*}{\partial y}\right\} \tag{4}$$

$$\overline{v_L} = \frac{1}{4\sigma}\text{Real}\left\{F_5 V_0\frac{\partial V_0^*}{\partial y} + F_6 U_0\frac{\partial V_0^*}{\partial x} + F_7 V_0\frac{\partial U_0^*}{\partial x}\right\} \tag{5}$$

where $*$ means the complex conjugate, F_5, F_6 and F_7 are expressed as

$$F_5 = -8i\exp\{-(1-i)\xi\} + 3(1+i)\exp\{-2\xi\} - 3 + 5i \tag{6}$$
$$F_6 = -4i\exp\{-(1-i)\xi\} + (1+2i)\exp\{-2\xi\} - 1 + 2i \tag{7}$$
$$F_7 = F_5 - F_6 \tag{8}$$

where $\xi = z_1/\delta$, z_1 is the distance away from the bottom and points normally into the inviscid region, $\delta(= \sqrt{2\nu/\sigma}$; ν is the kinematic viscosity) the thickness of the boundary layer.

With the known expressions of U_0, V_0 or U_0^*, V_0^* in Eqs.(2) and (3), Lagragian mass transport velocities $\overline{u_L}$, $\overline{v_L}$ in the bottom boundary layer in Eqs.(4)and(5) can be evaluated.

2.3 The sediment transport rate model

From the sediment transport field, the development of the topographical change or the local scouring around structures is calcurated by the continuity equation for the sediment given as

$$\frac{\partial h(x,y;t)}{\partial t} = \left\{ \frac{\partial q_x(x,y;t)}{\partial x} + \frac{\partial q_y(x,y;t)}{\partial y} \right\} \tag{9}$$

in which h is the above–mentioned still water depth, q_x and q_y are the sediment transport rates in volume of material per unit time and width in the $x-$ and $y-$ directions, respectively.

Consider the sediment transported in the $s-$ direction by mass transport $V(= \sqrt{\overline{u_L}^2 + \overline{v_L}^2})$, as shown in Fig. 1. The sediment transport model q_s proposed by Watanabe(1981) is widely used in and out the surf zone.

$$q_s = \frac{A_1 w_f}{(1 - \lambda_0)s_0 g\sqrt{s_0 g d_{50}}}(u_*^2 - u_{*c}^2)u_* \tag{10}$$

in which A_1 represents dimensionless parameter, w_f the sediment settling velocity, λ_0 the porosity of the bed material, s_0 the specific weight of the sediment in water, d_{50} the median diameter of the sediment, u_* the friction velocity and u_{*c} the critical shear velocity.
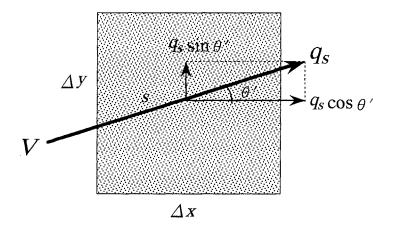

Fig. 1 Simplified model of the sediment transport rate

The sediment transport rate of Eq. (10) is generally based on the sediment transport rate of Eq. (10) is generally based on the sediment transported by breaking wave over the slope bed. Therefore, Eq. (10) is applied to the sediment transport over the plane bed like the present study, the sediment transport rate may be overestimated. Consequently, the new model for the sediment transport applicable to the cases that the spatial change of the wave height is dominant, is proposed on the approximation described in the following.

Equation (10) can be approximated by

$$q_s \sim u_*^3/g \sim V_{bmax}^3/g \sim \frac{H^3}{gT^3 \sinh^3 kh} \tag{11}$$

where $V_{bmax} = \sqrt{(U_b^2 + V_b^2)|_{max}}$, T is the period of the incident wave, k the wave number.

Similarily, the mass transport velocity V can also be approximated as follows.

$$V \sim \frac{1}{\sigma}U_{0s}\frac{\partial U_{0s}}{\partial s} \sim \frac{H^2}{gT^3 \sinh^3 kh} \tag{12}$$

where U_{0s} indicates the water particle velocity in the s–direction near the bed.

The following Eq. (13) is obtained by combining Eq. (11) with (12).

$$q_s \sim VH \tag{13}$$

Equation (13) means that the sediment transport rate is proportional to VH. The wave height H in the vicinity of large scale structures changes largely in space due to the scattered wave superimposed on the incident wave, and since the wave height H corresponds to the dynamic pressure, its magnatude represents the extent of the sediment suspension. From this point of view, it seems to be more reasonal that the wave height H is explicitly included in the sediment transport rate. In the present study, consequently, the sediment transport rate q_s at an equilibrium state is given as

$$q_s = \frac{A}{1-\lambda_0}(\Psi_m - \Psi_c)VH \tag{14}$$

where A indicates the dimensionless parameter, $\Psi_m (= f_w V_{bmax}^2/(2s_0 g d_{50})$; f_w is the wave friction factor) the Shields parameter, Ψ_c the critical Shields parameter.

In calculating Eq. (14), the wave height H is evaluated with Eq. (1), the water particle velocities U_0 and V_0 are evaluated with Eqs. (2) and (3) using

the source distribution function method, and the mass transport velocities $\overline{u_L}$ and $\overline{v_L}$ are also evaluated with the values $(U_0, V_0, U_0^*$ and $V_0^*)$ by means of Eqs. (4) and (5).

2.4 Topographical change at an equilibrium state

It is assumed that the wave field has little change after the bottom profile change, that is, the sediment transport rates at the equilibrium condition can be evaluated with those $q_x(x, y; 0)$, $q_y(x, y; 0)$ at $t=0$, and the acting time T_c of wave when the bottom topography reaches an equilibrium state is determined from the experimental results, since the present study aims to establish the simple method that is able to predict the topographical change, the local scouring depth around structures.

From Eq. (9),

$$
\begin{aligned}
\triangle h_c(x, y) &= \int_0^{t_c} \left\{ \frac{\partial q_x(x, y; t)}{\partial x} + \frac{\partial q_y(x, y; t)}{\partial y} \right\} dt \\
&\cong \left\{ \frac{\partial q_x(x, y; 0)}{\partial x} + \frac{\partial q_y(x, y; 0)}{\partial y} \right\} T_c \\
&= \left\{ \frac{\partial(q_s \cos \theta')}{\partial x} + \frac{\partial(q_s \sin \theta')}{\partial y} \right\}_{t=0} T_c
\end{aligned}
\tag{15}
$$

in which, $\triangle h_c(x, y)$ repesents the change of the still water depth, and $\triangle h_c > 0$, $\triangle h_c < 0$ and $\triangle h_c = 0$ correspond to, respectively, the scouring, the doposition and no–change. Eq. (14) is applied to Eq. (15) to evaluate $\triangle h_c$. The pattern of the bottom configuration around structures is divided into three parts such as the scouring area $(\triangle h_c > 0)$, the deposition area $(\triangle h_c < 0)$ and no change area $(\triangle h_c = 0)$.

2.5 Numerical computation

In Eq. (14), the values of the dimensionless parameter A, the porosity of the bed material λ_0, the specific weight of the sediment in water s_0, and the critical Shields parameter Ψ_c, respectively, were taken as $0.02 \sim 0.05$, 0.4, 1.65, and 0.08 for the relatively fine sand $(d_{50}=0.015\text{cm})$ and 0.07 for the relatively coarse sand $(d_{50}=0.038\text{cm})$. Then, the mass transport velocity V at a midle point $(\xi=1/2)$ within the boundary layer were used. In the case of the wave friction factor f_w, Eq. (16) presented by Swart(1974) was applied.

$$
f_w = \exp\{-5.977 + 5.213(a_m/k_s)^{-0.194}\}
\tag{16}
$$

in which a_m is the amplitude of the orbital motion at the bottom, k_s the bed roughness and took the median diameter d_{50} of sand.

In calculating Eq. (15), $T_c=5200 \times T$ was chosen from the experimental results as will be mentioned later.

3 Laboratory experiments

3.1 Dimensional anaysis

Taking the structures installed in a line with the same diameters into consideration, the non–dimensional bottom configuration change $\Delta h_c/H_I$ around the three large cylindrical structures at an equilibrium state is mainly governed by the following 9 parameters.

$$\frac{\Delta h_c}{H_I} = \phi_1 \left\{ \frac{r}{D}, \theta, \frac{D}{L}, \frac{e_1}{D}, \frac{e_2}{D}, \alpha, \frac{H_I}{L}, \frac{h}{L}, \frac{d_{50}}{L} \right\} \qquad (17)$$

where r is the radial distance, θ the clockwised angle along the structures measured from the first point of the structures where the incident wave contacts, e_1 the distance between structures I(the right one from the incident wave) and II(the center one), e_2 the distance between structures II and III(the left one) and α the incident wave angle. $E_2/D = \infty$ corresponds to the case of two structures and $e_1/D = e_2/D = \infty$ does to one structure. In the present paper, the effects of the following 6 parameters on the topographical change are mainly discussed.

$$\frac{\Delta h_c}{H_I} = \phi_2 \left\{ \frac{r}{D}, \theta, \frac{D}{L}, \frac{e_1}{D}, \alpha, \frac{d_{50}}{L} \right\} \qquad (18)$$

3.2 Experimental equipments and conditions

Laboratory experiments were carried out in a wave basin(28m in length, 11m in width and 0.8m in depth) with a flat bottom. A piston-type wave generator was installed at one end and the wave dissipating sandy beach with the slope of 1/10 was constructed at the other end. And the wave absorbing filters were set up on the both sides of the basin to diminish wave reflection from side walls as small as possible. The surface piercing cylindrical structures with the same diameters, were installed in a line on a sandy bed(400cm in length 500cm in width and 7cm in depth). Test conditions for the movable bed are listed in

Table 1 Test conditions for the topographical change

D (cm)	d50 (cm)	h (cm)	T (s)	Hi (cm)	α (deg.)	e1/D	e2/D	n
47.2	0.015	20	1.4	5.7	0	1.0	∞	2
					0	2.0		
					0	3.0		
					22.5	1.0		
					45			
					67.5			
					90			
	0.038				0	1.0		
					0	2.0		
					0	3.0		
					22.5	1.0		
					45			
					67.5			
					90			
90	0.015				0	1.0		
					45			
	0.038				0			
					45			
47.2	0.015				0		1.0	3
					45			
	0.038				0			
					45			
47.2	0.015					∞	∞	1
	0.038							
90	0.015							
	0.038							

Table 1, in which n means the number of structures. The experimental waves satisfied with the live bed state for all the cases, were continuously generated until the bottom topographical change seemed to close to an equilibrium state. The bottom topographical changes were carefully measured with point gauges at all the 2cm–interval mesh points within the sandy bed. The water particle velocities near the bottom and water surface profiles around the structures were measured with electromagnetic type velocity meters and capacitance–type wave gauges, respectively, for the same conditions as the movable bed ones to examine the validity of the employed theory regarding the wave kinematics and the wave heights.

4 Results and discussion

4.1 Topographical change around structures

Figure 2 represents the time evolution t/T of the non–dimensional topographical change $\Delta h/H_I$ at four locations where the comparatively larger scouring depth occurred. In Fig. 2, x' is the offshoreward distance measured from the structure surface. As shown in Fig. 2, it can be judged that the number t/T of waves reached the equilibrium state is approximately more than 5000,
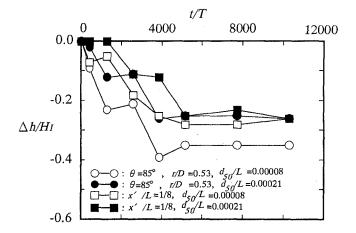

Fig. 2 Time evolution of the topographical change
$(D/L = 0.26, e_1/D = 1.0, H_I/L = 0.03, h/L = 0.11, \alpha = 0°)$

regardless of the places and the sediment sizes. This result is almost the same as that of Xie(1981) in front of breakwarer, or of Katsui and Toue(1992) around one large cylinder. In the present paper, the topographical change at $t/T=5200$ is taken to be the equilibrium state, and the experimental results at $t/T=5200$ are compared with the computed ones(Eq. (15) with $T_c=5200 \times T$).
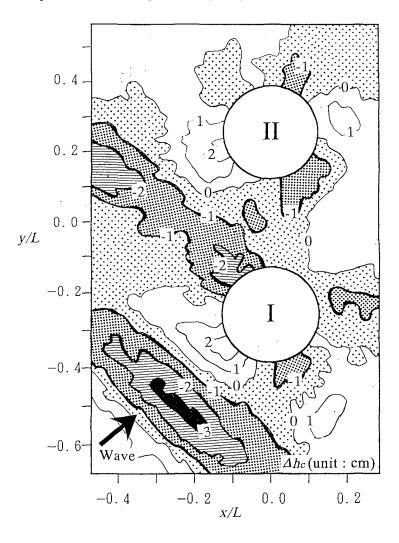

Fig. 3(a) Topographical change around two structures
$(D/L = 0.26, e_1/D = 1.0, H_I/L = 0.03, h/L = 0.11, \alpha = 45°, d_{50}/L = 0.00008)$

In general, the bottom configuration, the local scouring area and its depth around cylindrical structure are changed according to the number of structures, the structure's diameter, the incident wave angle and the sediment size.
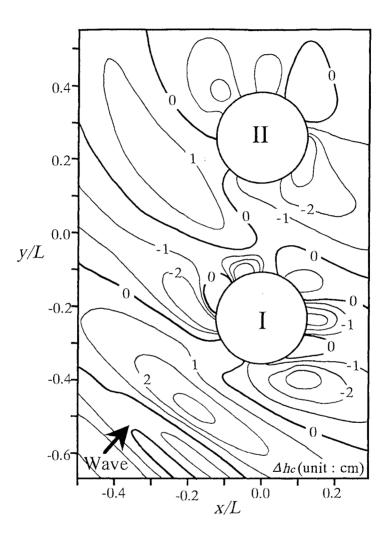

Fig. 3(b) Topographical change around two structures(computed)
$(D/L = 0.26, e_1/D = 1.0, H_I/L = 0.03, h/L = 0.11, \alpha = 45°, d_{50}/L = 0.00008)$

Figure 3(a) and (b), respectively, show the experiment result and the computed one of the bottom configuration Δh_c around the two structures in the case of $\alpha = 45°$, $e_1/D = 1.0$ and $D/L = 0.26$. In Fig. 3(a) and (b), the digits indicate the values of the topographical change Δh_c, and the signs of $-$ and $+$, respectively, indicate the scouring(black area in Fig. 3(a))and the deposition(white area in Fig. 3(a))). Experiments with the sediment size of $d_{50} = 0.038$cm in place of $d_{50} = 0.015$cm were also conducted and their results were reported by Kim and Iwata(1993). In the case of the relatevely fine sediment(this study), the scouring depth and its area are larger and wider than those of the case of the relatevely coarse one(Kim and Iwata, 1993). In the cases of obliquely incident waves like $\alpha = 45°$, since the onshore structure II is located at the sheltered area of the offshore strucure I, a little change or no change is generally found around onshore structure I. Comparing the experimental result with the computed one, it is seen that the bottom configuration around structures can be well estimated with the present theory.

4.2 Topographical change along structures

Figure 4 illustrates the non-dimensional topographical change $\Delta h_c/H_I$ at $r/D = 0.53$ along the structures with parameter of e_1/D. In Fig. 4, the solid line represents the experimental result and the dashed line the computed one. The maximum scouring depth takes place at $\theta = 45° \sim 135°$(see Fig. 4 and 5) and in Fig. 4, the maximum scouring depth becomes smaller in order of $e_1/D = 1.0$(Fig. 4(a)), $e_1/D = 3.0$(Fig. 4(b)) and $e_1/D = \infty$(Fig. 4(c)). It is inferred that the influence of diffracted wave from one structure on the other one can not be neglected for $e_1/D = 3.0$. It is also seen that theoretically estimated values are in good agreement with experiments.

Figure 5 shows the effect of the sediment size on the non-dimensional topographical change $\Delta h_c/H_I$ for the case of $D/L = 0.49$. When the sediment size is smaller(see Fig. 5(a)), the scouring depth and its area are larger and wider, as mentioned above. And the maximum scouring depth for the case of larger diffraction parameter $D/L = 0.49$(see Fig. 5(a)) is larger than that of smaller one $D/L = 0.26$(see Fig. 4(a)). The reason for this is inferred as follows. When the D/L becomes large, the spatial difference of the wave height H also becomes large. As explained before, the sediment is easy to be suspended and to be transported due to mass transport velocity and its large change in space caused by the large difference of the wave height H in space. Consequently, the scouring depth for the case of larger diffraction parameter becomes larger.
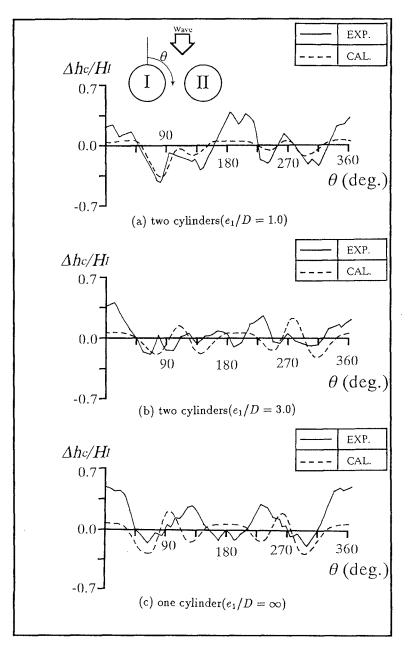
Fig. 4 Topographical change along structures
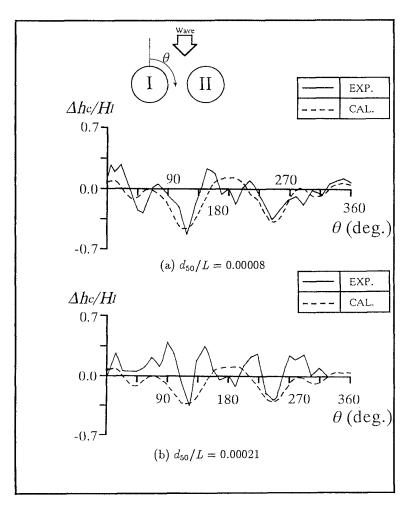$(D/L = 0.26, H_I/L = 0.03, h/L = 0.11, \alpha = 0°, d_{50}/L = 0.00008, r/D = 0.53)$

Fig. 5 Topographical change along two structures
$(D/L = 0.49, e_1/D = 1.0, H_I/L = 0.03, h/L = 0.11, \alpha = 0°, r/D = 0.53)$

5 Concluding remarks

The bottom configuration changes around cylindrical structures under wave actions have been discussed. Main conclusions obtained in the present study are summarized as follows.

(1) The bottom configuration, the local scouring area and its depth around cylindrical structure are changed according to the number of structures, the structure's diameter, the incident wave angle and the sediment size.

(2) The bottom topographical change around structures can be well evaluated with the present theory.

(3) Under the obliquely incident wave, the scouring depth along the offshore structure I is larger than that along the onshore structure I.

(4) With increasing of the diffraction parameter D/L, the scouring depth becomes larger.

References

Carter, T. G., P. L. F. Liu and C. C. Mei(1973) : Mass transport by waves and offshore sand bedforms, J. of Waterways, Harbours and Coastal Eng. Div., ASCE, Vol. 99, pp. 165–184.

Isaacson, M. Q.(1979) : Wave induced forces in the diffraction regime, in Mechanics of Wave–Induced Forces on Cylinders, ed. T. L. Shaw, Pitman, London, pp. 68–89.

Katsui, H. and T. Toue(1992) : Evaluation of the scouring depth around a large scale offsore structure, Proc. 39th Coastal Engg. Conf., pp. 496–500(in Japanese).

Kim, C.-J. and K. Iwata(1993) : Local Scouring around Two Large Circular Cylinders, Proc. 25th IAHR, Vol.3, pp. 159–166.

Kim, C.-J., T. Sanada, A. Imai, Y. Miyaike and K. Iwata(1994) : Wave field around multiple large cylindrical structures, Proc. 41st Coastal Engg. Conf., pp. 351–355(in Japanese).

Swart, D. H.(1974) : Offshore transport and equiliblium profiles, Pub. No. 131, Delft Hydr. Lab., 244pp.

Watanabe, A(1985) : Nearshore dynamics and coastal processes, edited by K. Horikawa, Univ. of Tokyo Press, pp. 272–284.

Xie, X. L.(1981) : Scouring patterns in front of the breakwaters, Coastal Engg. Group, Dep. of Civil Engg., Delft University of Technology, 61p.